New Ideas for Understanding the Structure and Magnetism in AgF_2: Prediction of Ferroelasticity

Inés Sánchez-Movellán,[a] Jorge Moreno-Ceballos,[a] Pablo García-Fernández,[a] Jose Antonio Aramburu,*[a] and Miguel Moreno[a]

Abstract: In the search for new high-temperature superconductors, it has been proposed that there are strong similarities between the fluoroargentate AgF_2 and the cuprate La_2CuO_4. We explored the origin of the possible layered structure of AgF_2 by studying its parent high-symmetry phase and comparing these results with those of a seemingly analogous cuprate, CuF_2. Our findings first stress the large differences between CuF_2 and AgF_2. Indeed, the parent structure of AgF_2 is found to be cubic, naturally devoid of any layering, even though Ag^{2+} ions occupy trigonal sites that, nevertheless, allow the existence of a Jahn-Teller effect. The observed *Pbca* orthorhombic phase is found when the system is cooperatively distorted by a local E⊗e trigonal Jahn-Teller effect around the silver sites that creates both geometrical and magnetic layering. While the distortion implies that two Ag^{2+}–F^- bonds increase their distance by 15% and become softer, our simulations indicate that covalent bonding and interlayer electron hopping is strong, unlike the situation in cuprate superconductors, and that, in fact, exfoliation of individual planes might be a harder task than previously suggested. As a salient feature, these results prove that the actual magnetic structure in AgF_2 is a direct consequence of vibronic contributions involved in the Jahn-Teller effect. Finally, our findings show that, due to the multiple minima intrinsic to the Jahn-Teller energy surface, the system is ferroelastic, a property that is strongly coupled to magnetism in this argentate.

Introduction

The existence of high-temperature (high-Tc) superconductivity in some layered oxocuprates has stimulated research on transition metal compounds containing different d^9 ions.[1–4] In these cases, the search for superconductivity is guided by the presence of three key ingredients found in the high-Tc cuprates, namely 1) a crystal lattice with layered structure, 2) the existence of elongated sixfold coordinated metal complexes often associated to the Jahn-Teller (JT) effect, and 3) a strongly antiferromagnetic (AFM) ground state in each of the metal planes.

In this hunt for new d^9-superconductors during the last two decades intense efforts[1–5] have been focused on the exploration of materials involving $4d^9$ Ag^{2+} cations. As this cation exhibits a higher electronegativity than Cu^{2+},[6] all known Ag^{2+} compounds are fluorides. Up to now one hundred stable Ag^{2+} compounds, such as AgF_2, Cs_2AgF_4 or $KAgF_3$,[1,2] have been synthesized. Moreover, in oxides,[7,8] chlorides[9–11] and bromides[10,12,13] the Ag^{2+} cation has been stabilized but only in the form of impurity. This handful of bulk materials have to be further dredged to find those that present an adequate layered AFM ground state.[1–5] Among these fluorides particular attention has been paid to the simple AgF_2 lattice, characterized by an unusually large oxidizing power.[14]

The structure of this compound is customarily[1,2,4,5,15] represented in the form shown in Figure 1, displaying stacked

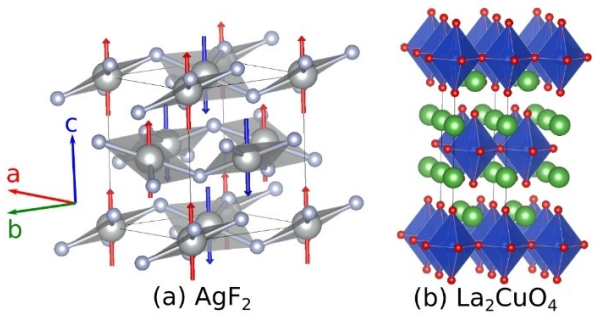

Figure 1. a) Usual representation (see, e.g., refs. [1], [2], [15]) of the layered structure of AgF_2 (silver ions in gray, fluorine ions in light blue) including red and blue arrows to represent, in a collinear fashion, the magnetic structure. It can be seen that an AFM coupling exists in the *ab*-plane. b) The structure of the parent compound for high-Tc superconductors, La_2CuO_4, showing the isolated layers containing elongated CuO_6 complexes (in blue) that are separated by LaO sheets (La^{3+} and O^{2-} ions are represented, respectively, as green and red spheres).

[a] I. Sánchez-Movellán, J. Moreno-Ceballos, Dr. P. García-Fernández, Prof. J. A. Aramburu, Prof. M. Moreno
Departamento de Ciencias de la Tierra y
Física de la Materia Condensada
Universidad de Cantabria
Avenida de los Castros s/n, 39005 Santander (Spain)
E-mail: aramburj@unican.es

Supporting information for this article is available on the WWW under https://doi.org/10.1002/chem.202101865

AgF_2 layers along the *c*-axis that host a strong, quasi-2D AFM order. It has been argued[5] that the key to unlock stronger AFM and, possibly, high-temperature superconductivity in this argentate is related with the internal geometry of these AgF_2 sheets. As can be seen in Figure 1 the layers are significantly buckled with vertex-sharing AgF_4 complexes assembled in alternating directions. Systematic analyses of the magnetic structure[5] indicate that flattening the geometry of these slabs would reinforce the AFM coupling allowing that found in the parent material of high-Tc, La_2CuO_4 to be surpassed. Moreover, based on first-principles simulations, it has been proposed[16] that these layers are surprisingly bound by weak van der Waals interactions with a cleavage energy that is comparable to that of graphite and, as a consequence, they should be easily exfoliable. In the same study, Xu et al.[16] find that in their free-standing configuration each individual AgF_2 sheet is still buckled but, due to the JT effect, they undergo a cooperative deformation into one of three equivalent minima separated by small energy barriers that provides the system with ferroelastic properties. Combined with the inherent anti-ferromagnetism of the system, they showed that bidimensional AgF_2 is a multiferroic material.

While previous works on AgF_2[1–5,14–18] focus on the layered nature of the system and the similarities with other quasi-bidimensional systems, like La_2CuO_4, there are still many open questions on the nature of the tridimensional crystal and the way the individual sheets and magnetism emerge in its bulk. For example, in layered perovskites like La_2CuO_4[19,20] magnetism is contained within CuO_2 atomic planes that are separated from each other physically by two LaO planes with certain likeness with the rock-salt structure (Figure 1). The difference in composition between CuO_2 and LaO planes also helps localizing electrons in their respective sheets, preventing inter-layer hopping. This clearly contrasts with the situation in AgF_2 where the composition is homogeneous and the origin of the layered structure is not a local change in the chemistry of the system. On the other hand, the claims of van der Waals bonding between AgF_2 sheets seem at odds with the strong bonding expected for the crystal. In fact, it is important to note that the single AgF_2 layer studied by Xu et al.[16] is more closely related to the hexagonal structure of bulk $CuCl_2$, basis of some graphite intercalation compounds (see, e.g., ref. [21]), than the orthorhombic lattice of AgF_2 shown in Figure 1. Thus, the production of AgF_2 layers, like the one studied in ref. [16], seems to be a much more involved process than the peeling-off graphene from graphite.

In this work we use density functional theory (DFT) calculations in order to discuss the origin of the apparently layered structure of AgF_2 and its connection with the magnetism of this system. In a first step, we prove the existence of a trigonal JT effect in AgF_2. In a second step, we show that crystalline and magnetic structures are strongly interconnected through the cooperative JT effect and that, due to the presence of this phenomenon, the system displays multiple equivalent minima leading to the emergence of ferroelasticity in the system. This shows that bulk AgF_2 is multiferroic, combining strongly intertwined magnetic and elastic properties.

Finally, in order to establish links and differences between argentates and cuprates we will analyze AgF_2 in parallel with CuF_2 (see also ref. [3]). We feel that this is a much closer analog to AgF_2 than La_2CuO_4 since this system avoids the presence of chemically foreign LaO sheets. In both (CuF_2, AgF_2) systems, and due to the localization of active d^9 electrons, it is crucial to know the origin of the local distortion and the nature of ground state of MX_6^{4-} complexes (M = d^9 ion, X = ligand), to understand their associated optical and magnetic properties.

The local distortion in compounds with d^9 cations, such as CuF_2,[2,22,23] K_2CuF_4,[24] or Cs_2AgF_4,[25,26] has widely been ascribed to an octahedral E⊗e JT effect despite the low symmetry displayed by such crystalline lattices. As the crystal structure of AgF_2 bears similarities with that of CuF_2 it has been assumed that the geometry of both compounds is the result of a JT distortion of the MF_6^{4-} units (M = Cu, Ag) giving rise to tetragonally elongated octahedra of D_{4h} symmetry with a hole in a $d_{x^2-y^2}$ type orbital.[2,3] Nevertheless, it has recently been shown, by means of first principles calculations, that CuF_6^{4-} complexes in CuF_2 actually exhibit a compressed geometry followed by an additional orthorhombic distortion that preserves a dominant $d_{3z^2-r^2}$ character for the hole a situation that is not due to the JT effect.[27] A similar pattern also holds for K_2CuF_4 or Cs_2AgF_4.[28]

Bearing these facts in mind, the present work aims to gain a better insight into the structure of AgF_2 and the ground state of AgF_6^{4-} units using DFT calculations. In order to achieve this goal, the present study is based on five fundamental steps: 1) To explore the structure of the so-called *parent phase* of Pbca AgF_2, formed when all open shell $4d^9$ Ag^{2+} cations are substituted by closed shell $4d^{10}$ Cd^{2+} ones, with similar ionic radii but a more spherical electronic density. Accordingly, the equilibrium geometry of the parent phase can display a higher symmetry than the observed one and be a good starting point for understanding the AgF_2 structure. 2) To analyze the behavior of a single Ag^{2+} impurity into the parent phase of the AgF_2 compound. 3) To study the cooperative effects analyzing the influence of the silver content on the lattice structure. 4) To carry out a parallel analysis of CuF_2 comparing the results obtained for copper and silver fluorides. 5) Once this matter is clarified, we will discuss the cooperative JT effect to highlight the relationship between local distortion and magnetism to show the presence of ferroelasticity and multiferroicity in AgF_2.

This work is organized as follows. Computational details of DFT calculations are shortly described in the next section, while main results of this work are displayed in the Results and Discussion. For the sake of clarity, we first apply the methodology to CuF_2 and subsequently to AgF_2. Some final remarks are provided in the last section.

Computational Methods

DFT periodic simulations on pure AgF_2 and its parent CdF_2 phase (either pure or doped with Ag^{2+}) were carried out using the Crystal17 code,[29] where Bloch wavefunctions are expanded as linear combinations of local functions which are, in turn, linear combinations of Gaussian type functions centered at atomic sites.[30]

It is worth noting that this code exploits at all steps of the calculations both translational invariance and point-symmetry of the crystals.[30]

In order to accurately perform both geometry optimizations and energy calculations, all ions were described by high-quality basis sets, specifically triple-ζ valence with polarization consistent basis optimized by Peitinger and coworkers,[31] which are provided by Crystal website.[29] The combination of these basis sets together with the hybrid exchange-correlation functional PW1PW, which includes 20% of Hartree-Fock exchange, has provided accurate crystal structures and properties for a wide range of different systems.[31,32]

As mentioned in the previous section, we have carried out geometry optimizations both on AgF_2, which belongs to the orthorhombic space group *Pbca*, and in a lattice where all Ag^{2+} ions have been replaced by closed shell Cd^{2+} ions (the parent phase), causing the system to undergo a phase transition to the parent cubic structure *Pa*-3 (see Results). These calculations were performed under the framework of spin unrestricted Kohn-Sham DFT, imposing tight convergence criteria for energy changes (10^{-9} a.u.) and RMS of gradient and atomic displacements (0.0001 a.u.). The integration in reciprocal space was carried out by sampling the Brillouin zone with 8x8x8 Monkhorst-Pack grid (that is the the distance between consecutive values of k according to the 3 reciprocal directions is 0.155, 0.142 and 0.135 $Å^{-1}$), which is enough to provide a full energy convergence. These results show great accordance between experimental and calculated distances in AgF_6^{4-} complex and lattice parameters. Both ferromagnetic (FM) and AFM states have been considered in the calculations, where we have noticed an increase in the energy per formula unit of 40 meV in the FM with respect to the AFM state at equilibrium.

Calculations on Ag^{2+}-doped CdF_2, where Ag^{2+} impurity initially occupies a Cd^{2+} lattice site on the parent phase Pa-3, were also performed. In these optimizations, atomic positions were relaxed within *Pbca* space group, keeping the lattice parameter of the parent phase fixed, which leads to a distorted AgF_6^{4-} complex. Primitive cell and 2x2x2 conventional supercell containing 12 and 96 ions, respectively, have been used, obtaining Ag^{2+}–F^- distances that are quite similar in both cases, with slight variations of less than 2%.

Additional energy calculations have been carried out for AgF_2, starting from the cubic *Pa*-3 structure and distorting the four AgF_6^{4-} complexes of the unit cell following a trigonal distortion, denoted as η. Then, lattice parameters have been relaxed in order to show how the previous distortion affects the global lattice structure, specifically cell vectors.

Results and Discussion

Seeking to explain the methodology employed in the analysis of crystal structures we first deal with the simpler case of CuF_2 which was previously investigated.[27] With these results in mind, we subsequently tackle the problem of AgF_2.

Structure and ground state of CuF_6^{4-} units in CuF_2

At normal conditions, CuF_2 exhibits a monoclinic structure with standard $P2_1/c$ space group that can be represented, alternatively, using the nonstandard $P2_1/n$ group,[22,23] which allows a distorted rutile structure to be identified (Figure 2).

As shown in Figure 2, the experimental geometry of CuF_6^{4-} units in CuF_2 involves an orthorhombically distorted octahedron where the three Cu^{2+}–F^- distances, $R_z = 1.917$ Å, $R_x = 1.932$ Å, and $R_y = 2.298$ Å and lattice parameters, measured at 4.2 K,[22] have previously been well reproduced by first principles calculations[27] (Table 1). The values of R_z and R_x at room temperature are coincident with those determined at 4.2 K while the length of the softest bond increases only by 0.5%.[22] Due to the closeness of R_x and R_z values that equilibrium geometry has been described in most scientific literature as the result of an octahedral JT effect leading to an elongated complex with y as main axis and a hole located in a x^2-z^2 type orbital.[2,22,23,33]

In order to have a closer look at this relevant issue, it is useful to calculate the parent (high-symmetry) structure of CuF_2. To achieve this goal, we replace all Cu^{2+} ions in CuF_2 by the closed shell Zn^{2+} ions, involving a more spherical electronic density, and then a geometry optimization is performed starting from the monoclinic $P2_1/c$ space group of CuF_2. The result of this process allows a reference, high-symmetry parent structure that can have a higher symmetry than $P2_1/c$ to be easily found.

The results obtained in this work for the parent phase of CuF_2 are also shown in Table 1. Upon the $Cu^{2+} \rightarrow Zn^{2+}$ substitution, the monoclinic $P2_1/c$ structure evolves until reaching the final tetragonal $P4_2/mnm$ space group characteristic of the stable phase of ZnF_2 at normal conditions[34] (Figure 1). Interestingly, the octahedron surrounding a Zn^{2+} cation involves two Zn^{2+}–F^- distances which are equal, $R_y = R_x =$ 2.041 Å, and is slightly compressed along the z-axis as $R_z =$

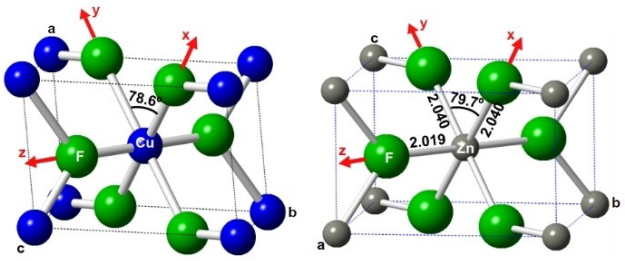

Figure 2. Units cells of the CuF_2 compound in the nonstandard monoclinic $P2_1/n$ setting (left) and ZnF_2 with tetragonal $P4_2/mnm$ space group (right). {*x*,*y*,*z*} are the local axes of the CuF_6^{4-} and ZnF_6^{4-} complexes. Experimental M–F (M = Cu, Zn) distances [Å] and F_x-M-F_y angles are also shown. The lattice parameters for ZnF_2 are $a = b = 4.707$ Å and $c = 3.128$ Å.

Table 1. Calculated values of metal-ligand distances R_x, R_y and R_z, and F_x-M-F_y (M = Cu, Zn) φ angles for CuF_2 and its parent phase. The values of three Cu^{2+}–F^- distances obtained for a Cu^{2+} impurity in the ZnF_2 lattice are also shown. Data corresponding to CuF_2 have previously been reported.[27]

System	Space group	R_z [Å]	R_x [Å]	R_Y [Å]	φ [°]
CuF_2	$P2_1/c$	1.918	1.936	2.265	77.6
parent phase (ZnF_2)	$P4_2/mnm$	2.007	2.041	2.041	78.6
ZnF_2:Cu^{2+}	$P4_2/mnm$	1.922	2.074	2.074	77.8

2.007 Å (Table 1). These values are essentially coincident with those measured at room temperature for ZnF_2[34] where $R_y = R_x = 2.040$ Å and $R_z = 2.019$ Å (Figure 2). Nevertheless, the local geometry around Zn^{2+} is not exactly tetragonal but D_{2h} because the F_x-Zn-F_y angle $\varphi \neq 90°$ (Figure 2 and Table 1).

Bearing these facts in mind, when a Cu^{2+} impurity replaces a Zn^{2+} cation of the ZnF_2 lattice the associated electronic ground state cannot be degenerate as there are no degenerate irreps in an orthorhombic D_{2h} local symmetry.[35] This fact thus practically excludes the existence of a JT effect in $ZnF_2:Cu^{2+}$. By contrast, the D_{2h} local geometry favors to place the hole of a Cu^{2+} impurity in a *singlet* a_g orbital with a dominant $3z^2$-r^2 character (Figure 2) lying mainly along the local *z*-axis. This conclusion is well supported by electron paramagnetic resonance (EPR) measurements carried out on $ZnF_2:Cu^{2+}$[36] which prove the absence of three equivalent distortions characteristic of a static Jahn-Teller effect.[9,27,37] Furthermore, if the ground state of CuF_6^{4-} units in ZnF_2 is A_g it can only be linearly coupled to fully symmetric A_g distortion modes and thus the $Zn^{2+} \rightarrow Cu^{2+}$ substitution does not give rise to a symmetry lowering, as observed in EPR data[36] and first principles calculations[27] (Table 1). Nonetheless, the replacement of a closed shell cation by Cu^{2+} with a hole in a mainly $3z^2$-r^2 orbital induces a reduction of R_z distance and a slight increase of $R_y = R_x$ ones that still preserves the local symmetry. This relaxation process, analyzed in ref. [37], can be clearly seen in our calculations (Table 1).

Upon increasing the Cu^{2+} concentration, when we actually deal with $Zn_{1-x}Cu_xF_2$ crystals and two adjacent Cu^{2+} can share some common ligands, an additional orthorhombic instability takes place in the *xy* plane in parallel to the $P4_2/mnm \rightarrow P2_1/c$ change of the lattice. This instability, well reproduced using supercells calculations, has previously been discussed in some detail.[27] In this distortion, the R_y distance increases while the R_x one decreases being then close, but not equal, to R_z (Table 1), that is, the system evolves weakening the two Cu^{2+}–F^- bonds along the *y*-axis but reinforcing the two x bonds. In this process, driven by a force constant which becomes negative,[38,39] the hole in the ground state preserves a dominant $3z^2$-r^2 character, although with a small x^2-y^2 mixing.[27] A similar orthorhombic instability takes place in A_2CuF_4 (A = K, Na) or Cs_2AgF_4.[28,37]

These facts thus show that neither the local distortion nor the ground state of CuF_6^{4-} units in the model compound CuF_2 can be explained through a JT effect despite the abundant literature assuming its existence.[2,22,33] Indeed, the force constant involved in a typical JT effect is positive[40] while the appearance of an asymmetric distortion obeys to an anisotropic electronic density which exerts a different force on the involved ligands. In the case of a d^9 ion under octahedral coordination such anisotropic density comes out when the hole is located in $\sim 3z^2$-r^2 or $\sim x^2$-y^2 orbitals thus leading to electronic densities that do not exhibit a cubic symmetry. More details on this matter are given in refs. [37] and [39].

Comparative study of AgF_2

In a similar way to what happens for CuF_2, in AgF_2 the cation is also sixfold coordinated (Figure 3). Nevertheless, AgF_2 exhibits a higher symmetry than CuF_2 as it is orthorhombic (space group Pbca) rather than monoclinic.[15] Calculated values of lattice parameters and Ag^{2+}–F^- distances (Table 2) coincide with experimental ones within 2%. It can be noticed that the Ag^{2+}–F^- distances along the *x*- (2.074 Å) and *y*- (2.067 Å) axes of Figure 3 are close but not equal while those for ligands along the *z*-axis are higher (2.584 Å). Moreover, the F–Ag–F angles in AgF_2 are not equal to 90°.

Using a similar process to that employed for CuF_2 we can try to elucidate the parent, high-symmetry structure that leads to the final, layered structure of AgF_2. In particular, we optimized the full geometry of the *Pbca* phase of AgF_2 when all the Ag^{2+} were replaced by closed-shell Cd^{2+} ions in order to eliminate distortions due to the anisotropic electronic shell of the Ag^{2+} ions. The results of the geometry optimization, displayed in Figure 4 and Table 3, show that the parent phase of AgF_2 is actually cubic and thus the substitution of Ag^{2+} by Cd^{2+} makes the lattice evolve from the orthorhombic *Pbca* to

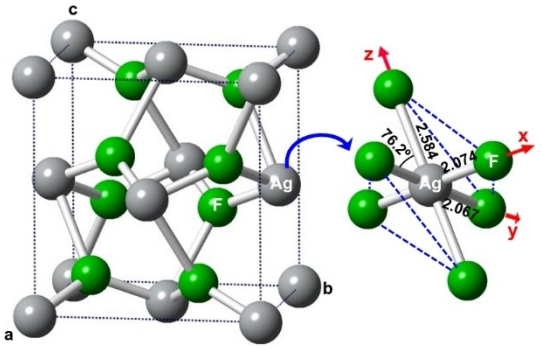

Figure 3. Unit cell of AgF_2 at ambient pressure, with an orthorhombic *Pbca* space group. One AgF_6^{4-} complex is also shown, where the R_x and R_y distances are slightly different, and the F–Ag–F angles are rather different from 90°. Dashed blue lines mark the two fluorine triangles distorted from equilateral ones in the parent cubic phase (Figure 4).

Table 2. Experimental[15] and calculated lattice parameters and metal-ligand distances for AgF_2. All values are in Å. Experimental values have been obtained at room temperature.

	a	*b*	*c*	R_z	R_x	R_y
experimental	5.073	5.529	5.813	2.584	2.067	2.074
calculated	5.178	5.622	5.766	2.618	2.094	2.096

Table 3. Optimized values of the lattice parameter, *a*, and Cd^{2+}–F^- distance, R(Cd^{2+}–F^-), for CdF_2 in two different phases. First row data corresponds to the *Pa*-3 parent phase of AgF_2, while second row data corresponds to the stable *Fm*-3*m* phase of CdF_2 at normal conditions displaying the fluorite structure. The different Cd^{2+} coordination number (CN) for both lattices is also shown.

System	Space group	Cd CN	*a* [Å]	*R*(Cd^{2+}–F^-) [Å]
parent phase of AgF_2	*Pa*-3	6	5.497	2.246
stable CdF_2	*Fm*-3*m*	8	5.393	2.335

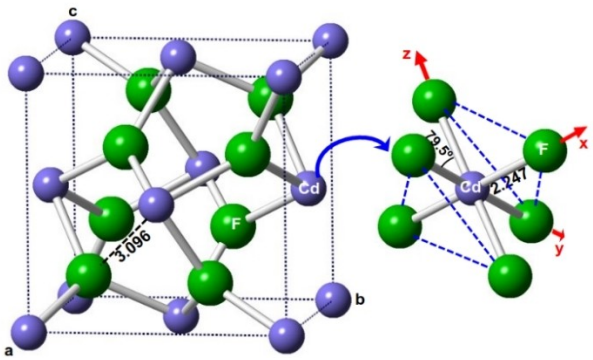

Figure 4. Left: Parent cubic *Pa*-3 phase of AgF_2 obtained by replacing Ag^{2+} with spherical Cd^{2+} ions. Right: D_{3d} flattened trigonal CdF_6^{4-} complex, where the top and bottom triangles (marked with dashed blue lines) are equilateral. In the cubic lattice, four of these trigonal complexes are placed in positions corresponding to a face-centered lattice but each oriented along one of the four main diagonals of the cube, leading to a *Pa*-3 structure.

the cubic *Pa*-3 space group. Nevertheless, even though the parent phase is cubic the fluorine coordination shell surrounding a Cd^{2+} is not a perfect octahedron as the F^--Cd^{2+}-F^- angles are rather different from 90° resulting in a flattened, trigonal CdF_6 complex (Figure 4). Even though the local symmetry is low, the trigonal axis of the complex surrounding each of the four Cd^{2+} ions in the motif is oriented along one of the four major diagonals of the cube leading to a global cubic symmetry of the system.

The structure of CdF_2 in the cubic *Pa*-3 phase looks rather similar to that of CdF_2 in the fluorite structure (cubic space group *Fm*-3 *m*) observed experimentally at normal conditions (Figure 5). Nevertheless, the coordination number for CdF_2 in the fluorite structure is eight while in the *Pa*-3 parent phase of AgF_2 it is only six. Thus, according to Pauling's rules,[41] the Cd^{2+}–F^- distance (Table 3) is a somewhat higher for the *Fm*-3 *m* phase (2.335 Å) than for the *Pa*-3 one (2.246 Å). At the same time, the change from eightfold to sixfold coordination implies that in the parent phase there are two Cd^{2+}–F^- distances at 3.096 Å reflecting the breaking of the corresponding bonds (Figure 4). This fact increases the lattice parameter of the *Pa*-3 phase with respect to that of the *Fm*-3 *m* structure as shown in Table 3.

It is worth noting that the calculated structure for the *Pa*-3 parent phase of AgF_2 is just the equilibrium structure at ambient pressure observed for $Cd_{0.5}Pd_{0.5}F_4$, where Cd^{2+} and Pd^{2+} ions occupy the same sites at 50%.[42] It was also claimed that one of the high-pressure phases of AgF_2 exhibits the same *Pa*-3 structure,[43] although this matter is still debated.[44]

A crucial point in the present analysis concerns the behavior of a single Ag^{2+} impurity in the *Pa*-3 parent phase. We have verified that under the $Cd^{2+}\rightarrow Ag^{2+}$ substitution, and maintaining fixed the position of the rest of lattice ions, the ground state of AgF_6^{4-} units is orbitally doubly degenerate. This result may in principle be surprising as the local symmetry of a Cd^{2+} ion in the parent *Pa*-3 phase is not octahedral O_h but trigonal D_{3d}.

However, if under a perfect octahedral symmetry the ground state of a AgF_6^{4-} unit is E_g the nature of the ground state remains twofold-degenerate after a descent in symmetry from O_h to D_{3d}.[35,40] Such an electronic doublet can also be preserved in lower trigonal symmetries like C_{3v} or C_3, while an E_g state in O_h *already* splits into A_{1g} and B_{1g} under a tetragonal perturbation.[35] Accordingly, the ground state under a D_{4h} symmetry is no longer degenerate thus excluding the existence of a JT effect, a matter well verified in cases like $K_2ZnF_4:Cu^{2+}$ or $Ba_2ZnF_6:Cu^{2+}$.[45,46] By contrast, under the $O_h\rightarrow D_{3d}$ symmetry descent the ground state of an AgF_6^{4-} unit in the parent phase is still degenerate and thus can experience a JT effect. The existence of a static JT effect under trigonal symmetry has been verified in cases like $ZnSiF_6\cdot 6H_2O:Cu^{2+}$,[47–49] $CdCl_2:M^{2+}$ (M = Cu, Ag)[10,50] or $CaF_2:Y^{2+}$.[51]

Despite the ground state of a d^9 ion in trigonal symmetry can still be degenerate there are differences with the behavior under a higher octahedral symmetry. So, considering the trigonal {*X*, *Y*, *Z*} coordinates depicted in Figure 6 there is no one but two pairs of d-wavefunctions belonging to the E_g irrep in D_{3d}.[40] Such pairs are simply described by {X^2-Y^2, 2*XY*} and {*XZ*, *YZ*} in the trigonal basis (Figure 6). Accordingly, the highest, partially occupied d-level of Ag^{2+} in AgF_2 involves a linear combination of *four* different d-wavefunctions. In the same vein, although in D_{3d} symmetry the JT effect gives rise to three adiabatic minima they do not exhibit a tetragonal symmetry

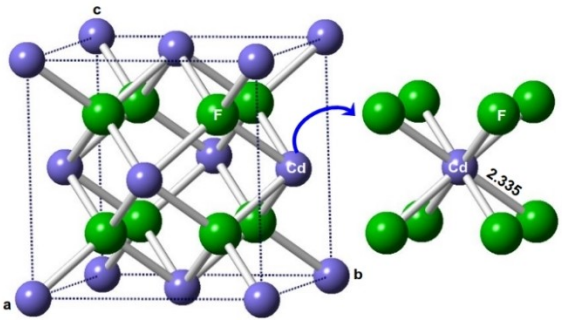

Figure 5. Stable cubic *Fm*-3 *m* phase of CdF_2 displaying the fluorite structure. It can be observed that the parent phase of AgF_2 shown in Figure 4 is strongly related to this structure.

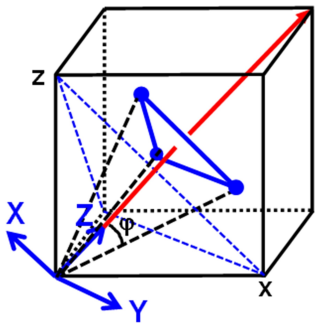

Figure 6. Description of {*X*,*Y*,*Z*} trigonal coordinates. In the {*x*,*y*,*z*} cartesian basis, the unit vectors along the *Z*, *Y* and *X* directions are expressed as *Z*(1/$\sqrt{3}$, 1/$\sqrt{3}$, 1/$\sqrt{3}$), *Y*(1/$\sqrt{2}$, −1/$\sqrt{2}$, 0) and *X*(−1/$\sqrt{6}$, −1/$\sqrt{6}$, 2/$\sqrt{6}$), respectively.

such as it happens when the initial, high-symmetry configuration is octahedral.

The equilibrium geometry corresponding to one of the adiabatic minima obtained for a single Ag^{2+} impurity is displayed in Table 4 and shown in Figure 7. Results are compared to experimental ones for AgF_2[15] and also to those calculated in this work for $NaF:Ag^{2+}$ where the initial geometry is octahedral.

The results on $NaF:Ag^{2+}$ are consistent with the EPR measurements by Monier et al.[52] proving the existence of an elongated geometry due to a static JT effect. This geometry is usually observed for d^9 impurities in cubic lattices and sixfold coordination[39,53] with the exception of $CaO:Ni^{+}$,[54] a matter discussed in ref. [55]. A geometry close to the elongated one in octahedral symmetry has also been observed when the host lattice is trigonal such as for $ZnSiF_6\cdot 6H_2O:Cu^{2+}$[47–49] or $CdCl_2:M^{2+}$ (M = Cu, Ag).[10,50]

These calculations for the Ag^{2+} impurity in *Pa*-3 CdF_2 lead to bond distances in the AgF_6^{4-} unit that are rather close to those derived for $NaF:Ag^{2+}$. However, it is important to note that while the F^--Cd^{2+}-F^- angles in the *Pa*-3 phase differ from 90° only by ≈10° the global shape of the flattened trigonal complex is significantly different from the octahedral case (Figures 4 and 7) and have important differences in the JT distortion of the complex.

Table 4. Equilibrium geometry corresponding to one of the adiabatic minima obtained for a single Ag^{2+} impurity in the sixfold coordinated *Pa*-3 CdF_2 lattice showing the relaxation effects. Results are compared to the experimental equilibrium values of AgF_6^{4-} units in pure AgF_2, derived at room temperature,[15] and also to those calculated in the cubic NaF lattice where the initial geometry around the impurity is O_h. $\langle R\rangle$ just means the average value of three metal–ligand distances. All distances are in Å.

System	R_z	R_x	R_y	$\langle R\rangle$
$NaF:Ag^{2+}$	2.399	2.114	2.114	2.209
$CdF_2:Ag^{2+}$	2.445	2.128	2.134	2.235
AgF_2 (experimental)	2.584	2.067	2.074	2.241

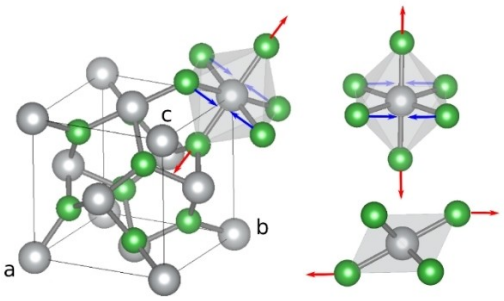

Figure 7. Distortion of one of the trigonal AgF_6^{4-} complexes of the parent high-symmetry *Pa*-3 phase of AgF_2. The faces of AgF_6^{4-} complexes go from being equilateral triangles in *Pa*-3 to acute triangles in the experimental *Pbca* structure. Notice that, unlike with the usual JT effect in octahedral systems, the elongation of the complex (red arrows) is not along the bond axis as it keeps the top and bottom faces of the complex parallel to each other. This can be clearly seen in the lateral view complex, on the right-bottom side of the figure, where the Ag–F bonds point in a different direction from the distortion (red) arrows.

As shown on Table 4, on passing from Ag^{2+}-doped CdF_2 to pure AgF_2 the value of the average metal-ligand distance, $\langle R\rangle$, is the same but the distortion increases. We have verified that this fact is related to the silver content of the lattice. For instance, if in the unit cell of the *Pa*-3 phase we replace three of four Cd^{2+} ions by Ag^{2+} we find elongated AgF_6^{4-} complexes whose metal-ligand distances (R_z = 2.532 Å, R_x = 2.077 Å and R_y = 2.146 Å) are closer to that found for pure AgF_2 (Figure 2 and Table 4). It is important to note that, at difference with the usual octahedral JT effect, in this case the distortion is not directly produced along the Ag–F bond axes but it is rather a distortion that changes the shape of the equilateral triangular faces of the complex, elongating them into acute triangular faces that remain parallel throughout the distortion (Figure 5). Nevertheless, the change from an equilateral to an acute triangle implies a reduction of the distance between two ligands and consequently that between them and the central cation (see blue arrows on the diagram on the right side of Figure 7).

Due to the perfect degeneracy at the initial geometry, a fingerprint of a JT effect in an octahedral unit is the existence of two different distortions whose energies are very close as they differ by an energy barrier, *B*, lying typically in the range 10–100 meV.[56] To explore this key issue, we have built a linear transformation that allows us to smoothly interpolate between the high-symmetry *Pa*-3 geometry of CdF_2 to the distorted *Pbca* minimum of AgF_2. We can further use this transformation to *extrapolate* the geometry to negative values of the distortion that in a usual JT system would correspond with the transition state between minima. In this process the distortion of a single complex can be characterized through a parameter η as follows

$$R_z = \langle R\rangle + 2\eta;\ R_x = R_y = \langle R\rangle - \eta \qquad (1)$$

We have calculated the energy associated with the Jahn-Teller deformation associated to η both in the fractional coordinates and the lattice parameters by using the information contained in Table 5. Using the two extrema presented in Table 5 and the geometry of the parent structure we can interpolate the geometries that allow the energy surfaces characteristic of a JT effect in Figure 8 to be plotted. There, we have verified that for both $\eta > 0$ and $\eta < 0$ branches a lower energy is always reached including the lattice relaxation.

If we designate by η_L the local distortion corresponding to the lowest energy value of a given branch, the equilibrium situation is obtained for the $\eta > 0$ branch with η_L = 0.16 Å and a JT stabilization energy E_{JT} = 193 meV, comparable to E_{JT} = 201 meV previously determined for $NaCl:Ag^{2+}$.[11]

Table 5. Description of local and lattice distortions associated with the lowest energy value for both $\eta > 0$ and $\eta < 0$ branches depicted in Figure 8. η_L is the local distortion of the AgF_6^{4-} unit corresponding to the lowest energy value of a given branch.

Branch	η_L [Å]	Relative energy [meV]	*a* [Å]	*b* [Å]	*c* [Å]
$\eta > 0$	0.16	0	5.138	5.544	5.847
$\eta < 0$	−0.10	88	5.715	5.320	5.372

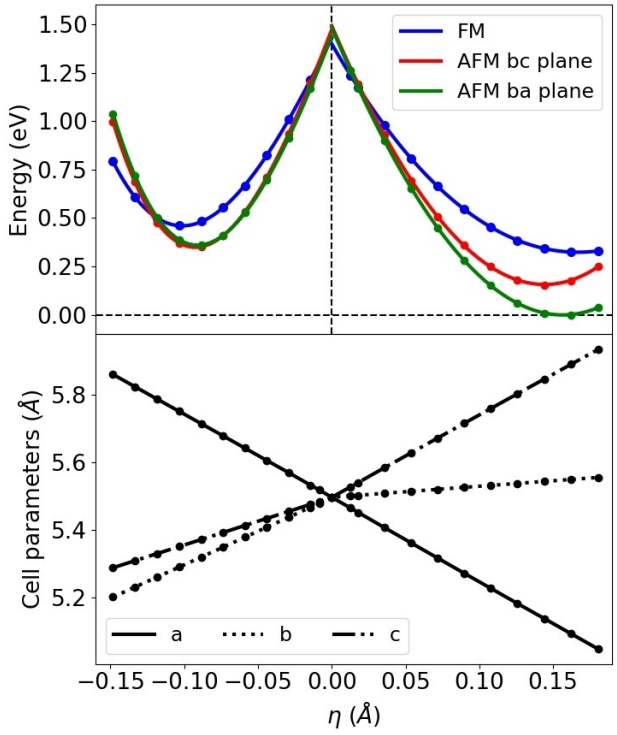

Figure 8. Top: Variation of the total energy of AgF_2 for the FM (blue line) and the AFM states along the planes *bc* (red line) and *ba* (green line) obtained by interpolating the geometries between the parent phase, $\eta = 0$, and the critical points with $\eta > 0$ and $\eta < 0$ (distorted structures) shown in Table 5. It can be seen that the shape of the curves is similar to that found for JT systems.[37,46] Bottom: Variation of the lattice parameters corresponding to the values of η of the JT energy curves presented at the top of the figure, showing the presence of ferroelasticity in the system and the strong coupling between the ground electronic state and the strain of the system. Note that the magnetic ground state depends on the distortion: it is FM for undistorted complexes ($\eta = 0$), but it is AFM (although oriented along different planes) for the distorted minima.

As shown on Figure 8, the lowest energy value in the $\eta < 0$ branch appears at $\eta_L = -0.10$ Å involving an energy barrier per single complex equal to $B = 88$ meV above the absolute minimum at $\eta_L = 0.16$ Å. This situation is thus akin to that found for d^9 impurities in cubic crystals under a static JT effect.[39,52,55] In these cases, with the known exception of $CaO:Ni^+$,[53,54] the equilibrium geometry corresponds to an elongated octahedron while the compressed geometry ($\eta < 0$) is located at an energy above the minimum equal to $B = 28$ meV for $NaF:Ag^{2+}$ or $B = 62$ meV for $NaCl:Ag^{2+}$.[11]

Layered structure, magnetism and ferroelasticity in AgF_2

After discussing the local distortions around the Ag^{2+} ion in AgF_2 we are in position to analyze the origin of the layered structure and subsequently the magnetism of this material.[5,57] Both AgF_2 phases, the parent cubic *Pa*-3 one (Figure 4) and the experimental orthorhombic *Pbca* (Figure 7), contain four vertex-sharing trigonal AgF_6^{4-} complexes positioned in a face-centered configuration. In the cubic *Pa*-3 phase, each of these complexes has its trigonal axis oriented along one of the four main diagonals of the cube. In the orthorhombic *Pbca* structure, the local distortion is equivalent on all complexes and extends one bond in the upper and lower faces of the flattened trigonal complexes (Figure 7) whose shape changes from equilateral triangle to acute one. Note that this transformation is quite different from the usual elongation of the octahedral complex in the cubic JT problem.

Considering the combined action of the local elongation of each of the trigonal complexes in the cubic lattice and their different orientation, we find that the resulting cooperative distortion produces an extension of bonds along one of the cubic lattice's cell vectors while keeping the length of another one roughly fixed and contracting the third one. We can observe this in detail by looking at the linear transformation from the cubic *Pa*-3 structure to the orthorhombic *Pbca* one represented in Figure 8. Here, we can see how the cell vectors relax with the distortion leading to the splitting of the cubic lattice parameter $a = 5.497$ Å into the contracted, roughly constant and extended lattice parameters ($a = 5.073$ Å, $b = 5.529$ Å and $c = 5.813$ Å, respectively) of the orthorhombic structure. This extension along one of the main cubic axes is the reason why AgF_2 is usually considered as a layered compound as the bonds along the orthorhombic *c*-axis are clearly weakened due to the cooperative JT effect. From a symmetry standpoint it is clear that the complexes can elongate equivalently along the three cubic axes and so the system may end up in one of three well-separated minima characteristic of the JT effect. This property shows that bulk AgF_2 is ferroelastic, a very usual property of many cooperative JT crystals (see, e.g., ref. [58]). The barrier between each of the configurations is, as reflected in Figure 8, 88 meV/unit formula, a value that could be tuned by the application of pressure or growing the lattice on a substrate.

From this point of view, when one considers AgF_2 as a layered system it is clear that the atomic sheets in this material are clearly different from those of a layered perovskite like La_2CuO_4 (Figure 1). In particular, AgF_6 complexes have short in-layer ($R \approx 2.13$ Å) and long inter-layer ($R \approx 2.58$ Å) bonds while in the perovskite the complexes are located exclusively on one layer. These differences are further reflected on the electronic structure. While in the layered perovskites the dispersion of the bands in the direction perpendicular to the layers is negligible, in AgF_2 the equivalent band dispersion (see the Supporting Information) is significant, clearly indicating that bond-length extension is not enough to destroy interlayer bonding. As mentioned in the introduction, Xu et al.[13] calculated a cleavage energy similar to that of graphite for AgF_2 leading to the conclusion that interlayer bonding is van der Waals. This conclusion does not stand with the analysis carried out here where we show that significant mixed ionic covalent bonding, typical of transition metal complexes, exists between layers and thus the role played by the longest Ag–F bonds at 2.58 Å cannot be neglected.

In order to look in more detail at this issue we have performed simulations on AgF_2 where the long cell parameter is extended to a very long distance (15 Å) and resulting structure

is relaxed. Interestingly, we have found that this process involves an increase of energy of 0.42 eV per unit formula which is thus similar to what is obtained in a similar transformation in NaCl (0.54 eV/unit formula). Thus, in both cases the energy turns out to be one order of magnitude larger to that of graphite (0.05 eV/unit formula). Furthermore, the final AgF_2 layer structure obtained by extending the lattice in one direction, where the silver complexes are nearly square planar, is quite different from the one considered by Xu et al.[13] where the complexes are flattened trigonal, as in bulk and systems like $CuCl_2$.[15] Thus, it seems that reaching the proposed nearly trigonal geometry by peeling-off one layer of AgF_2 would be difficult as the necessary rearrangement of atoms involves overcoming significant energy barriers.

Coming, finally, to the determination of the magnetic structure and its correlation with the JT distortion discussed above, it can be noticed that in the cubic *Pa*-3 phase no AFM state has pure cubic symmetry. This state, that in a cubic perovskite is realized as the AFM–G state where an ion with its magnetic moment pointing up (or down) is completely surrounded along the three main axes of the crystal by magnetic ions where the spin points down (respectively up). By contrast in AgF_2 the antiferromagnetic coupling cannot be produced along the three main axes of the crystal, implying frustration, that is, in the first coordination sphere of an ion there are always magnetic moments that are parallel and antiparallel to the central one. In fact, for $\eta = 0$ (cubic *Pa*-3 phase), the FM state is lower in energy than any AFM state, as shown in Figure 8. This magnetic frustration is broken when the JT effect comes into play and produces an elongation of one of the axes of the lattice and a contraction along the other one. Observing Figure 8 we can see that the existence of the JT distortion plays a key role for stabilizing an AFM coupling between two Ag^{2+} ions separated by a short bond (Ag–F distance of 2.07 Å) and involving an Ag–F–Ag angle of 130°. This conclusion is underpinned by experimental findings.[57] Moreover, the present results lead to a weak FM coupling for two Ag^{2+} ions separated by a long bond (Ag–F distance of 2.58 Å) and involving an Ag–F–Ag angle of 118°, which is also in agreement with experiments.[57] These results are consistent with the usual behavior of superexchange interactions favoring AFM coupling on FM one 1) the stronger the bond is, and 2) the more linear the metal–ligand–metal bond is.[59,60]

Moreover, we can study the change in the direction of the AFM planes with the JT distortion. Indeed, as can be observed in Figure 8, as the AgF_6 complexes go from an elongated (acute triangular faces, $\eta > 0$) to a compressed (obtuse triangular faces, $\eta < 0$) configuration, the direction of the elongation/compression of the lattice axes switches from *a* to *c* axes. This process is accompanied with a change of the order of the AFM states of the system. When $\eta > 0$ ($c > b > a$) the ground state shows AFM coupling in the *ba* plane, that is, the green line is the ground state, while this coupling occurs in the *bc* plane when $\eta < 0$ ($c < b < a$; the red line is the ground state). These results thus stress that the actual magnetic structure in AgF_2 is a direct consequence of vibronic contributions involved in the JT effect. Indeed, as shown in Figure 8, vibronic effects lead to energy shifts of ~0.2 eV per complex while the energy change induced by varying the magnetic structure is one order of magnitude lower.

Conclusions

In this work, we have shown that the geometry and magnetic structures of AgF_2, usually referred in the literature[1–5,14–18] as a layered silver analog to high-temperature cuprate superconductors, are a direct consequence of the cooperative Jahn-Teller effect in this lattice. This is an important difference from the layered structures of cuprates like La_2CuO_4, where the origin of the layers is chemical, as CuO_2 planes are separated from each other by rock-salt LaO planes. In fact, it was proven that the parent phase of this argentate is cubic (*Pa*-3 group), where symmetry prevents the appearance of any layers. The Jahn-Teller distortions taking place in the lattice, while significant, are far from strong enough to destroy interlayer band dispersion. In cuprates, the interlayer band dispersion is almost completely quenched due to the strong barriers created to electron hoping due to a region with a different composition from that of the CuO_2 atomic sheets. Moreover, we have shown that interlayer bonding has a strong mixed ionic/covalent character that contrasts with previous suggestions of van der Waals bonding.[16] Another consequence of the Jahn-Teller origin of the geometry of the system is that AgF_2 is a ferroelastic system in which the distortion-induced strain is directly connected with and controls the direction of antiferromagnetic coupling, a signal of consistent multiferroic behavior.

Finally, we would like to stress the importance of symmetry when analyzing the properties of a system. Although CuF_2 and AgF_2 would, at first sight, seem relatively similar,[2,3,57] the different symmetry of the parent phase, tetragonal and cubic, respectively, leads to quite different behavior. In CuF_2, the tetragonal symmetry of the parent phase already excludes the existence of a Jahn-Teller effect, while a true degeneracy exists in the parent phase of AgF_2 giving rise to many interesting features characteristic of the Jahn-Teller effect in solids, like ferroelasticity and multiferroicity. Moreover, the nature of the three-minimum Jahn-Teller energy surface found in the flattened trigonal AgF_6^{4-} complexes of AgF_2 is quite different from that in systems where the symmetry of AgF_6^{4-} complexes is *initially* octahedral. In fact, the distortion in the trigonal D_{3d} complex always occurs in the same plane, breaking the third-order axis of the system, while in the octahedral (O_h) one, the distortions take place in orthogonal directions along metal–ligand bonds. Understanding these delicate differences are key to correctly predicting the properties of these systems.

Supporting Information

The Supporting Information contains the DFT-calculated band structure of AgF_2 and La_2CuO_4.

Acknowledgements

The support by the Spanish Ministerio de Ciencia, Innovación y Universidades under Project PGC2018-096955-B-C41 and the European Union and the University of Cantabria under FEDER project EQC2019-006136-P is acknowledged.

Conflict of Interest

The authors declare no conflict of interest.

Keywords: cuprates · Jahn-Teller effect · quantum magnetism · silver fluorides · superconductivity

[1] W. Grochala, *J. Supercond. Novel Magn.* **2018**, *31*, 737–752.
[2] Z. Mazej, D. Kurzydłowski, W. Grochala in *Photonic and Electronic Properties of Fluoride Materials* (Eds.: A. Tressaud, K. Poeppelmeier), Elsevier, Amsterdam, **2016**, pp. 231–260.
[3] C. Miller, A. S. Botana, *Phys. Rev. B* **2020**, *101*, 195116.
[4] X. Yang, H. Su, *Sci. Rep.* **2014**, *4*, 5420.
[5] J. Gawraczynski, D. Kurzydłowski, R. A. Ewings, S. Bandaru, W. Gadomski, Z. Mazej, G. Ruani, I. Bergenti, T. Jaron, A. Ozarowski, S. Hill, P. J. Leszczynski, K. Kamil Tokar, M. Derzsi, P. Barone, K. Wohlfeld, J. Lorenzana, W. Grochala, *Proc. Nat. Acad. Sci.* **2019**, *116*, 1495–1500.
[6] J. A. Aramburu, M. Moreno, *Solid State Commun.* **1986**, *58*, 305–309.
[7] L. A. Boatner, R. W. Reynolds, M. M. Abraham, Y. Chen, *Phys. Rev. Lett.* **1973**, *31*, 7–10.
[8] P. García-Fernández, A. Trueba, M. T. Barriuso, J. A. Aramburu, M. Moreno, *Phys. Rev. Lett.* **2010**, *104*, 035901.
[9] J. Sierro, *J. Phys. Chem. Solids* **1967**, *28*, 417–422.
[10] T. Miyanaga, *J. Phys. Soc. Jpn.* **1978**, *46*, 167–175.
[11] A. Trueba, J. M. Garcia-Lastra, C. de Graaf, P. García-Fernández, M. T. Barriuso, J. A. Aramburu, M. Moreno, *Chem. Phys. Lett.* **2006**, *430*, 51–55.
[12] M. Yamaga, Y. Hayashi, H. Yoshioka *J. Phys. Soc. Jpn.* **1979**, *47*, 677–678.
[13] J. A. Aramburu, M. Moreno, *Solid State Commun.* **1987**, *62*, 513–516.
[14] W. Wegner, K. Tokar, J. Lorenzana, M. Derzsi, W. Grochala, *W. Phys. Chem. Chem. Phys.* **2020**, *22*, 21809–21815.
[15] P. Fisher, D. Schwarzenbach, H. M. Rietveld, *J. Phys. Chem. Solids* **1971**, *32*, 543–550.
[16] X. Xu, Y. Ma, T. Zhang, C. Lei, B. Huang, Y. Dai, *Nanoscale Horiz.* **2020**, *5*, 1386–1393.
[17] A. Grzelak, J. Gawraczyński, T. Jaroń, D. Kurzydlowski, Z. Mazej, P. J. Leszczyński, V. B. Prakapenka, M. Derzsi, V. V. Struzhkin, W. Grochala, *Dalton Trans.* **2017**, *46*, 14742–14745.
[18] A. Grzelak, J. Gawraczyński, T. Jaroń, D. Kurzydlowski, A. Budzianowski, Z. Mazej, P. J. Leszczyński, V. B. Prakapenka, M. Derzsi, V. V. Struzhkin, W. Grochala, *Inorg. Chem.* **2017**, *56*, 14651–14661.
[19] R. Hord, G. Cordier, K. Hoffmann, A. Buckow, G. Pascua, H. Luetkens, L. Alff, B. Albert, *Phys. Rev. B* **2010**, *82*, 180508.
[20] P. Garcia-Fernandez, M. Moreno, J. A. Aramburu, *J. Phys. Chem. C* **2014**, *118*, 7554–7561.
[21] M. Suzuki, I. Suzuki, C. R. Burr, D. G. Wiesler, N. Rosov, K. I. Koga, *Phys. Rev. B* **1994**, *50*, 9188–9199.
[22] P. Fischer, W. Haelg, D. Schwarzenbach, H. Gamsjaeger, *J. Phys. Chem. Solids* **1974**, *35*, 1683–1689.
[23] T. Chatterji, Th. Hansen, *J. Phys. Condens. Matter* **2011**, *23*, 276007–276015.
[24] D. Reinen, *Inorg. Chem.* **2012**, *51*, 4458–4472.
[25] S. E. McLain, M. R. Dolgos, D. A. Tennant, J. F. C. Turner, T. Barnes, T. Proffen, B. C. Sales, R. I. Bewley, *Nat. Mater.* **2006**, *5*, 561–566.
[26] D. Kurzydłowski, T. Jaroń, A. Ozarowski, S. Hill, Z. Jaglicic, Y. Filinchuk, Z. Mazej, W. Grochala, *Inorg. Chem.* **2016**, *55*, 11479–11489.
[27] J. A. Aramburu, M. Moreno, *Inorg. Chem.* **2019**, *58*, 4609–4618.
[28] J. A. Aramburu, P. García-Fernández, N. R. Mathiesen, J. M. Garcia-Lastra, M. Moreno, *J. Phys. Chem. C* **2018**, *122*, 5071–5082.
[29] CRYSTAL basis sets. https://www.crystal.unito.it/basis-sets.php (accessed on January 22, 2021).
[30] R. Dovesi, et al. *CRYSTAL17 User's Manual* (University of Torino, Torino), **2017**.
[31] M. F. Peintinger, D. V. Oliveira, T. J. Bredow, *J. Comput. Chem.* **2013**, *34*, 451–459.
[32] T. Bredow, A. Gerson, *Phys. Rev. B* **2000**, *61*, 5194–5201.
[33] P. Reinhardt, M.-P. Habas, R. Dovesi, I. de P. R. Moreira, F. Illas, *Phys. Rev. B* **1999**, *59*, 1016–1023.
[34] T. Chatterji, M. Zbiri, T. C. Hansen, *Appl. Phys. Lett.* **2011**, *98*, 181911.
[35] M. Tinkham, in *Group Theory and Quantum Mechanics*, Mc Graw-Hill, **1964**.
[36] J. D. Swalen, B. Johnson, H. M. Gladney, *J. Chem. Phys.* **1970**, *52*, 4078–4086.
[37] I. Sanchez-Movellan, J. A. Aramburu, M. Moreno, *Phys. Chem. Chem. Phys.* **2020**, *22*, 7875–7887.
[38] I. Bersuker, *Chem. Rev.* **2013**, *113*, 1351–1390.
[39] J. M. Garcia-Lastra, M. T. Barriuso, J. A. Aramburu, M. Moreno, *Chem. Phys.* **2005**, *317*, 103–110.
[40] F. S. Ham in *Electron Paramagnetic Resonance* (Ed.: S. Geschwind), Plenum, New York, **1972**.
[41] L. Pauling in *The Nature of Chemical Bond*, 3rd ed., Cornell University, Ithaca (New York), **1960**, p. 538.
[42] B. G. Müller, *J. Fluorine Chem.* **1982**, *20*, 291–299.
[43] B. G. Müller, *Naturwissenschaften* **1979**, *66*, 519–520.
[44] J. Romiszewski, W. Grochala, L. Z. Stolarczyk, *J. Phys. Condens. Matter* **2007**, *19*, 116206.
[45] J. M. Garcia-Lastra, J. A. Aramburu, M. T. Barriuso, M. Moreno, *Phys. Rev. Lett.* **2004**, *93*, 226402.
[46] J. A. Aramburu, P. García-Fernández, J. M. García-Lastra, M. Moreno, *J. Phys. Chem. C* **2017**, *121*, 5215–5224.
[47] B. Bleaney, K. D. Bowers, R. S. Trenam, *Proc. R. Soc. London Ser. A* **1955**, *228*, 157–166.
[48] L. S. Dang, R. Buisson, F. I. B. Williams, *J. Physique (Paris)* **1974**, *35*, 49–65.
[49] J. A. Aramburu, A. Bhowmik, J. M. García-Lastra, P. García-Fernández, M. Moreno, *J. Phys. Chem. C* **2019**, *123*, 3088–3101.
[50] M. Hasayhi, H. Nakagawa, H. Matsumoto, *Memoirs of the Faculty of Engineering Fukui University* **1978**, *26*, 15–27.
[51] H. Bill, G. Magne, C. Balestra, D. Lovy *J. Phys. C* **1986**, *19*, L19-L23.
[52] A. Monnier, A. Gerber, H. J. Bill, *Chem. Phys.* **1991**, *94*, 5891–5896.
[53] H. Bill in *The Dynamical Jahn-Teller Effect in Localized Systems* (Eds: Y. E. Perlin, M. Wagner), Elsevier, Amsterdam, **1984**.
[54] W. Low, J. T. Suss, *Phys. Lett.* **1963**, *7*, 310–312.
[55] J. A. Aramburu, P. Garcia-Fernandez, J. M. Garcia-Lastra, M. Moreno, *ChemPhysChem* **2016**, *17*, 2146–2156.
[56] P. Garcia-Fernandez, A. Trueba, M. T. Barriuso, J. A. Aramburu, M. Moreno, *Prog. Theor. Chem. Phys.* **2011**, *23*, 105–142.
[57] P. Fisher, G. Roult, D. Schwarzenbach, *J. Phys. Chem. Solids* **1971**, *32*, 1641–1647.
[58] M. A. Augustyniak-Jabłokow, Y. V. Yablokov, K. Łukaszewicz, A. Pietraszko, V. E. Petrashen, V. A. Ulanov, *Chem. Phys. Lett.* **2001**, *344*, 345–351.
[59] P. W. Anderson, *Phys. Rev.* **1950**, *79*, 350–356.
[60] P. J. Hay, J. C. Thibeault, R. Hoffmann, *J. Am. Chem. Soc.* **1975**, *97*, 4884–4899.

Manuscript received: May 27, 2021
Accepted manuscript online: July 23, 2021
Version of record online: August 18, 2021

